Electrodeposited Nanolaminated CoNiFe Cores for Ultracompact DC–DC Power Conversion

Jooncheol Kim, Minsoo Kim, Florian Herrault, *Senior Member, IEEE*, Jae Y. Park, *Member, IEEE*, and Mark G. Allen, *Fellow, IEEE*

***Abstract*—Laminated metallic alloy cores (i.e., alternating layers of thin film metallic alloy and insulating material) of appropriate lamination thickness enable suppression of eddy current losses at high frequencies. Magnetic cores comprised of many such laminations yield substantial overall magnetic volume, thereby enabling high-power operation. Previously, we reported nanolaminated permalloy ($Ni_{80}Fe_{20}$) cores based on a sequential electrodeposition technique, demonstrating negligible eddy current losses at peak flux densities up to 0.5 T and operating at megahertz frequencies. This paper demonstrates improved performance of nanolaminated cores comprising tens to hundreds of layers of 300–500-nm-thick CoNiFe films that exhibit superior magnetic properties (e.g., higher saturation flux density and lower coercivity) than permalloy. Nanolaminated CoNiFe cores can be operated up to a peak flux density of 0.9 T, demonstrating improved power handling capacity and exhibiting 30% reduced volumetric core loss, attributed to lowered hysteresis losses compared to the nanolaminated permalloy core of the same geometry. Operating these cores in a buck dc–dc power converter at a switching frequency of 1 MHz, the nanolaminated CoNiFe cores achieved a conversion efficiency exceeding 90% at output power levels up to 7 W, compared to an achieved permalloy core conversion efficiency below 86% at 6 W.**

***Index Terms*—DC–DC power conversion, eddy current loss suppression, electroplated CoNiFe, nanolaminated core, sequential electrodeposition.**

I. Introduction

SATISFYING the ongoing trend of portable devices toward further size reduction and multifunctionality requires development of miniaturized dc–dc converters. One major challenge to such miniaturization is shrinking the physical size of passive components such as inductors and transformers; these components are typically much larger than active silicon devices such as MOSFETs and controllers [1]–[3]. Since the required inductance for dc–dc conversion is inversely proportional to the operation frequency, increasing the switching frequency results in physical size reduction of the passive components [4]. The size of the inductor can be further reduced by utilizing appropriate magnetic cores such as ferrites and metallic alloys. However, use of the magnetic cores may cause frequency-dependent magnetic losses (i.e., hysteresis and eddy current losses) and magnetic saturation that limit the power conversion efficiency and power handling capacity of converters [5]. In particular, metallic alloy cores that typically have high conductivity can suffer from significant eddy current losses when the thickness exceeds the skin depth of the material, limiting effective magnetic thickness to a few microns at the low megahertz frequency. Total core thicknesses in this range are likely not sufficient for high power handling ($>$10 W).

In order to simultaneously achieve both large effective magnetic thickness (for high power handling) and suppressed eddy current losses at high frequency (for physical size reduction), magnetic cores comprised of laminated thin metallic alloy films is a promising solution. The laminated cores are structured as alternating layers of sufficiently thin magnetic material (e.g., less than the skin depth of the material) to suppress eddy currents, and insulating material that prevents interlamination electrical current flow that would, otherwise, allow the eddy current to reestablish, resulting in an overall core magnetic thickness sufficient for high power handling. Sputtering is often used to develop laminated cores comprising tens of layers of thin laminations, due to its capability to deposit both magnetic materials (e.g., CoZrTa [6] and CoFeO [7]) and high resistivity to insulating material (e.g., SiO_2); but its relatively slow deposition rate and internal stress restrict the total achievable core thickness. While sputtering provides relatively simple deposition of laminated magnetic cores, electrodeposition generally requires additional steps to develop interlamination insulating layers since electrodeposition is typically performed with low resistivity (e.g., less than 50 $\mu\Omega \cdot$ cm) materials. However, electrodeposition is still an attractive fabrication technique as it preserves the attractive features of sputtered films (CMOS compatibility, batch fabrication, and ease of precise patterning via photolithography), while also enabling desirable core thicknesses at low equipment capital cost. These features enable the realization of power supply in package and power supply on chip [8]–[10]. Thus, there have been many attempts to realize laminated magnetic cores based on electrodeposition [11]–[15]. Recently, we have reported nanolaminated permalloy cores comprising tens to hundreds of layers of submicron-thick permalloy films based on automated sequential electrodeposition [16]. The developed core operated with negligible eddy

Manuscript received June 25, 2014; revised September 15, 2014; accepted October 21, 2014. Date of publication November 6, 2014; date of current version April 15, 2015. This work was supported by the Advanced Research Projects Agency-Energy under the Agile Delivery of Electrical Power Technology Program under Award DE-AR0000107. Recommended for publication by Associate Editor C. R. Sullivan.

J. Kim and M. Kim are with the Department of Electrical and Computer Engineering, Georgia Institute of Technology, Atlanta, GA 30332 USA (e-mail: jkim611@gatech.edu; mkim354@gatech.edu).

F. Herrault was with the Department of Electrical and Computer Engineering, Georgia Institute of Technology, Atlanta, GA 30332 USA. He is now with HRL Laboratories, Malibu, CA 90265 USA (e-mail: floherrault@gmail.com).

J. Park is with the Department of Electronic Engineering, Kwangwoon University, Seoul 139-701, Korea (e-mail: jaepark@kw.ac.kr).

M. G. Allen was with the Electrical and Computer Engineering, Georgia Institute of Technology, Atlanta, GA 30332 USA. He is now with the Department of Electrical and Systems Engineering, University of Pennsylvania, Philadelphia, PA 19104 USA (e-mail: mallen@upenn.edu).

Color versions of one or more of the figures in this paper are available online at http://ieeexplore.ieee.org.

Digital Object Identifier 10.1109/TPEL.2014.2368140

current losses in the megahertz frequency up to a peak operation flux density of 0.5 T, while achieving sufficiently large effective magnetic thickness for high (6 W) power handling.

In this paper, the sequential electrodeposition technique is applied to a new magnetic material with improved intrinsic magnetic properties (e.g., higher saturation flux density and lower coercivity) with the goal of developing nanolaminated magnetic cores with higher power handling capacity and lower volumetric magnetic loss than permalloy cores. These new material cores are characterized and demonstrated in a buck power converter application, and their performance is compared with previous permalloy cores.

II. Electrodeposited Thin Film Alloys

The selection of an appropriate electrodeposited alloy for the magnetic core is based on two intrinsic magnetic properties: 1) high saturation flux density (B_s), which may enable operation at high fluxes to achieve ultimate compactness of the magnetic components; and 2) low coercivity (H_c) to minimize magnetic hysteresis losses.

For typical toroid-shape inductive components, the maximum energy that can be stored in a closed magnetic field is expressed as

$$E = \frac{1}{2}Li^2 = \frac{1}{2}L\left(\frac{N\emptyset}{L}\right)^2 = \frac{1}{2}\cdot\frac{\emptyset^2}{\mu}\cdot\frac{l}{A} = \frac{1}{2}\frac{B_s^2}{\mu}\cdot A\cdot l \quad (1)$$

where L is the inductance [H], i is the applied current [A], $\emptyset$ is the peak magnetic flux [Wb], B_s is the saturation flux density [T], μ is the permeability [H/m], N is the number of winding turns, and l and A are the average circumference and cross-sectional area of the toroid [m and m^2]. Thus, the ultimate achievable energy density at a given frequency becomes [17]

$$E_d = \frac{1}{2}\cdot\frac{B_s^2}{\mu} \quad (2)$$

Consequently, the ultimate achievable power from a magnetic core at a given frequency can be estimated as

$$P_{\text{core}} = E_d\cdot V_{\text{core}}\cdot f = \frac{B_s^2\cdot V_{\text{core}}\cdot f}{2\cdot\mu} \quad (3)$$

where V_{core} is the volume of the magnetic core [m^3], and f is the operation frequency [Hz]. Therefore, high saturation flux density is critical for such inductor cores to preserve required power in a reduced device dimension, improving the ultimate achievable miniaturization of inductive components.

The volumetric magnetic hysteresis loss is expressed as [17], [18]

$$P_{V,\text{hyst}} = f * \oint HdB \quad (4)$$

where the cyclic integral is taken around the B–H loop, and f is the frequency at which the loop is traversed. Such loops are typically measured at low frequency. There can be changes in effective coercivity and permeability as frequency increases. However, assuming that the shape of the hysteresis loop throughout the entire frequency range of interest is invariable, the volumetric magnetic hysteresis loss at the operation flux density and frequency can be estimated as [18]

$$P_{V,\text{hyst}} = \frac{2\cdot f\cdot S\cdot B^2}{\mu} \quad (5)$$

where B is the operation flux density [T], and S is the shape factor that depends on the coercivity of the material. Therefore, desirable characteristics of magnetic metallic alloys for use as an inductor core should include high saturation flux density for high-power density devices as well as low coercivity for minimized magnetic hysteresis losses.

TABLE I
Properties of Electrodeposited Magnetic Materials Used as an Inductor Core

Magnetic Materials	B_s [T]	H_c [Oe]	ρ [$\mu\Omega\cdot$cm]	μ_r
$Ni_{80}Fe_{20}$ [8]	0.8	1.9	46	3000
$Ni_{80}Fe_{20}$ [16]	1.25	1.5	30	400
$Ni_{45}Fe_{55}$ [19]	1.5	0.5	45	280
$Ni_{50}Fe_{50}$ [13]	1.45	1	30	800
$Co_{89.3}Fe_{10.7}$ [20]	1.64	10.7	25	600
$Co_{83.2}Fe7Cu_{9.8}$ [20]	1.46	2.8	15	400
$Ni_{85}Fe_{14}Mo_1$ [21]	1.02	0.3	20	2200
$Co_{60}Ni_{15}Fe_{25}$ [22]	2.2	2.4	30	250
$Co_{44}Ni_{37}Fe_{19}$ (This work)	1.83	0.5	40	700

Properties of reported thin metallic alloy films used as inductor cores are presented in Table I. These materials are typically binary or ternary alloys of nickel, iron, and cobalt, with varying compositions showing saturation flux density of 1–2 T and coercivity less than 3 Oe. These properties are superior to those of conventional ferrites.

Among these candidates, electrodeposited CoNiFe has been utilized as a new lamination material in this paper since it exhibits high saturation flux density ($\sim$2 T) and low coercivity ($<$2 Oe) simultaneously. The developed nanolaminated CoNiFe cores comprise tens to hundreds of CoNiFe lamination layers, each layer having a thickness of 300–500 nm, which is far below the skin depth ($\sim$3 μm at 10 MHz) of the material. The superior performance of such a nanolaminated CoNiFe core includes not only realization of a large magnetic volume with suppressed eddy current losses but also exploitation of the superior magnetic properties of CoNiFe (i.e., high saturation flux density and low coercivity) enabling high power density capability and minimized magnetic hysteresis losses.

III. Fabrication of Nanolaminated CoNiFe Cores

The CoNiFe electrodeposition conditions (i.e., bath compositions and electroplating parameters) for this paper are adopted from [23]–[25] and modified for multilayer deposition as presented in Table II. The additives (i.e., sodium saccharin and sodium lauryl sulfate) play important roles for deposition stress relief and ionic mass transfer improvement throughout the multiple layers of electrodeposition. From an EDX (Hitachi, S-3700 VP-SEM EDX analyzer) measurement, the atomic composition of films electrodeposited as described in Table II was observed to be 44%-cobalt, 37%-nickel, and 19%-iron. Fig. 1 shows typical B–H hysteresis curves of electrodeposited CoNiFe films

TABLE II
ELECTRODEPOSITION CONDITIONS

Component	Quantity
$CoSO_4 \cdot 7H_2O$	0.08 [mol/L]
$NiSO_4 \cdot 6H_2O$	0.2 [mol/L]
$FeSO_4 \cdot 7H_2O$	0.03 [mol/L]
NH_4Cl	0.3 [mol/L]
Boric acid	0.4 [mol/L]
Sodium saccharin	2.1 [g/L]
Sodium lauryl sulfate	0.01 [g/L]
Temperature	23–25 °C
pH	2.7–2.9
Current density	20 [mA/cm^2]

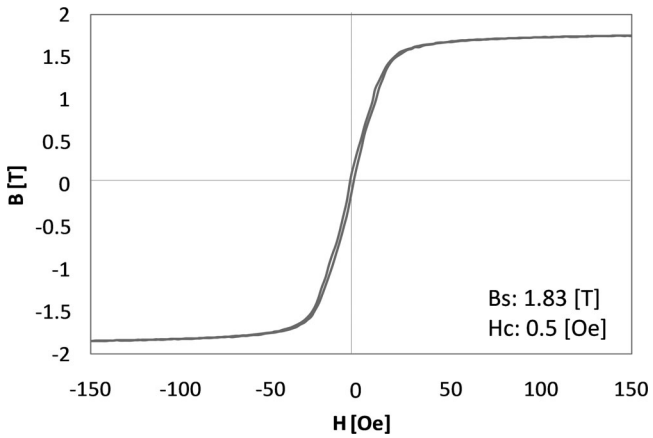

Fig. 1. Measured B–H hysteresis curves of electrodeposited CoNiFe.

using a vibrating sample magnetometer (VSM) (LakeShore, 7300 VSM) demonstrating saturation flux density of 1.83 T and coercivity of 0.5 Oe; these results correspond with the result from [24] and [25]. The higher saturation flux density and lower coercivity of CoNiFe compared to previously reported permalloy (1.25 T and 1.5 Oe) suggest higher power handling capability and lower intrinsic magnetic losses (e.g., hysteresis loss) of nanolaminated CoNiFe cores in compact power conversion.

In order to develop toroidal CoNiFe/copper multilayer magnetic cores, alternating CoNiFe and copper layers are sequentially deposited onto a sputtered copper seed layer on 4-in Si wafer through a lithographically patterned toroidal photoresist mold. Alternating sequential electrodeposition is carried out by an automated robot arm that moves between CoNiFe and sacrificial copper baths until the desired number of layers is achieved. The thickness of a single layer is precisely controlled by adjusting the electrodeposition time [26]. A commercial copper bath (Grobet, Clean Earth Cu-mirror solution) containing brighteners and levelers has been utilized for the sacrificial copper electrodeposition, providing a smooth surface topology for subsequent layers. Fig. 2(a) shows 3-D and cross-sectioned schematics of toroidal CoNiFe/copper multilayer structures after sequential electrodeposition. In this step, the core comprises alternating CoNiFe and copper layers in which eddy current losses are dominant due to the electrical connection between magnetic CoNiFe layers. In the next step, the sacrificial copper layers

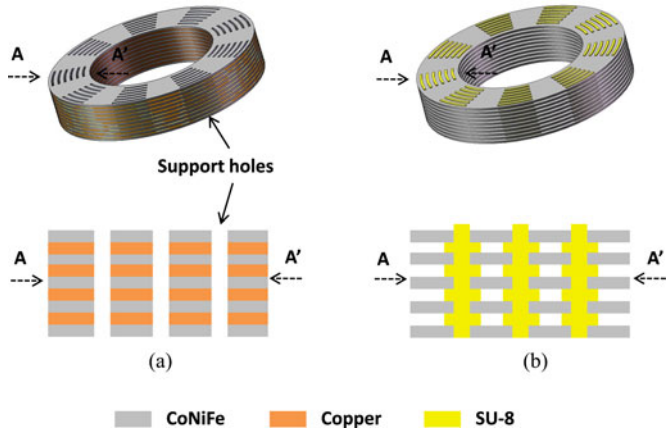

Fig. 2. Schematics of toroid multilayer CoNiFe core. (a) Before sacrificial copper layer etching and (b) after sacrificial copper layer etching.

are selectively removed, while insulating SU-8 polymer infiltrates between each CoNiFe lamination through support holes, forming the toroidal CoNiFe/air multilayer core as shown in Fig. 2(b). More details for the fabrication process are presented in [16]. In the CoNiFe/air multilayer structure, eddy currents are suppressed in the electrically insulated CoNiFe nanolaminations. SU-8 polymer supports individual CoNiFe nanolaminations, providing mechanical integrity of the multilayer core.

Fig. 3 shows various images of nanolaminated toroidal CoNiFe cores comprising 70–150 CoNiFe laminations with single-layer thickness of 300–500 nm. Fig. 3(a) shows optical images of batch-fabricated nanolaminated CoNiFe cores with outer diameter of 10 mm and inner diameter ranging from 6 to 8 mm. The dimensions and shapes of the toroids are precisely designable through lithographic patterning of photoresist. Fig. 3(b) shows a magnified top view demonstrating the support holes filled with SU-8. Fig. 3(c) and (d) shows cross-sectional SEM images of the finished core with SU-8 support and completely etched copper. The core comprises 150 layers of CoNiFe film with single-lamination thickness of 300 nm. Note that some lamination damage (e.g., compression or collapse) was observed during the cross sectioning process. Fig. 3(e) and (f) shows a side view of a nanolaminated core comprising 70 layers of CoNiFe film with single-lamination thickness of 500 nm.

IV. CHARACTERIZATION OF NANOLAMINATED CONIFE CORES

In order to characterize the performance of the nanolaminated CoNiFe cores, test inductors are prepared by placing the cores in laser-machined polymeric bobbins and winding them with wire as shown in Fig. 4. The test inductor fabrication procedure consists of: 1) laser micromachining of polymeric bobbin with desired number of notches for winding guide [see Fig. 4(a)]; 2) placing nanolaminated CoNiFe core in the bobbin [see Fig. 4(b)]; and 3) winding the bobbin with wire [see Fig. 4(d)]. An air core inductor is formed by winding the same bobbin without the magnetic core as shown in Fig. 4(c). The bobbin not only provides mechanical support for the nanolaminated core and winding but also allows reproducible windings through equally distributed notches.

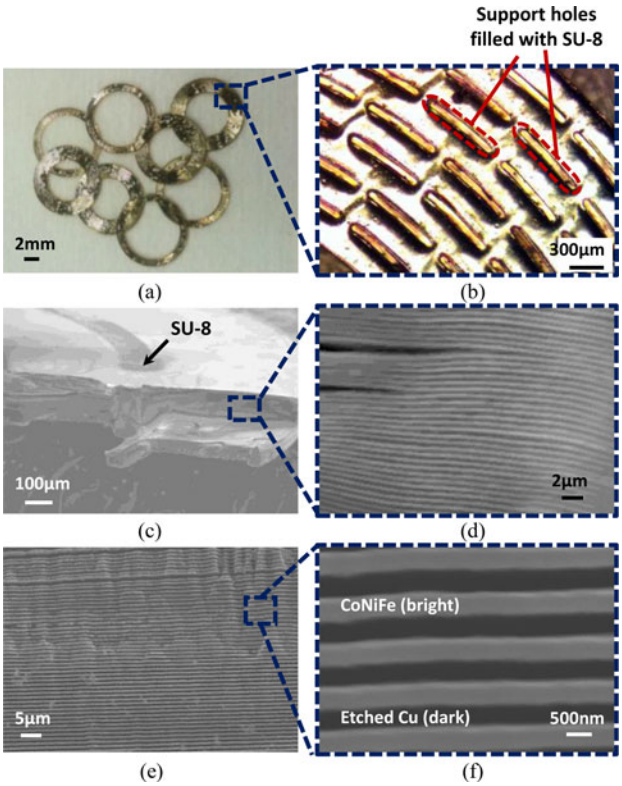

Fig. 3. Optical and SEM images of multilayer toroidal CoNiFe cores. (a) Batch-fabricated nanolaminated CoNiFe cores. (b) Magnified top view of the core showing support holes filled with SU-8. (c) Cross-sectional SEM image of fabricated core comprising 150 layers of 300-nm-thick CoNiFe films. (d) Magnified view of (c) showing copper layers are completely etched. (e) Side view of nanolaminated core comprising 70 layers of 500-nm-thick CoNiFe films. (f) Magnified view of (e).

Once the test inductors are prepared, three different types of characterizations are performed on the test inductors consecutively: 1) low flux *in situ* characterization using an impedance analyzer; 2) high flux characterization under large signal ac flux conditions; and 3) system level characterization in dc–dc converters. The result from each characterization is compared with the performance of the nanolaminated permalloy core with the same geometry.

For the reliable characterization of the nanolaminated cores, it is the first priority to ensure the isolation of each CoNiFe lamination since the core comprises tens to hundreds of 300–500-nm-thick CoNiFe layers. Measuring frequency-dependent core inductance *in situ* during the sacrificial copper layer etch is an effective method to validate the isolation of each CoNiFe nanolamination [16], which is challenging to verify by imaging due to the high lateral aspect ratio of the core. This *in situ* measurement enables the observation of inductance decrease as a function of frequency prior to the complete copper etch since any electrically connected CoNiFe layers form a bulk metallic core ($\sim$100 μm thickness) causing significant eddy current flow; this eddy current is manifested as an inductance decrease at higher frequencies. Consequently, one can infer the effective isolation of each CoNiFe lamination and, therefore, the suppression of eddy currents, when a constant inductance as a function of frequency is observed over the frequency range of interest.

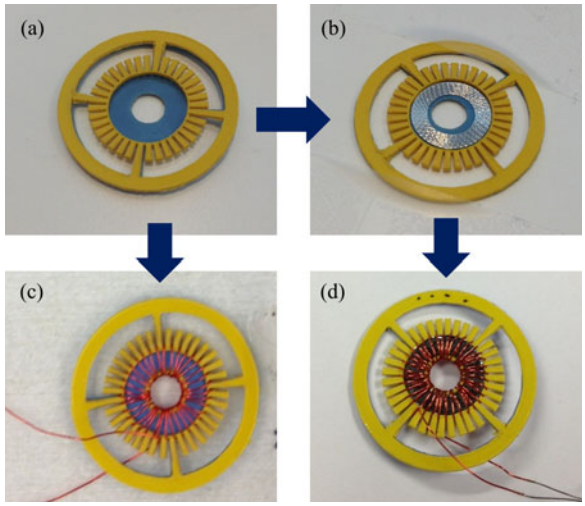

Fig. 4. Inductor fabrication steps. (a) Laser-micromachined polymeric bobbin. (b) Nanolaminated CoNiFe core placed in the bobbin. (c) 36-turn air core inductor. (d) 36-turn inductor with nanolaminated CoNiFe core.

Once the constant inductance as a function of frequency is observed from the low flux *in situ* measurement, the high flux characterization is carried out on the test inductor under large signal ac flux conditions. Since CoNiFe possesses higher saturation flux density than commercial ferrites, it is worthwhile to investigate the magnetic performance of nanolaminated CoNiFe core under simultaneous high flux and high frequency (HFHF) conditions. The HFHF test enables not only the assessment of maximum magnetic flux handling capacity but also the analysis of total core losses by decomposing it into hysteresis and eddy current components.

Finally, the test inductor is investigated in a dc–dc converter system with appropriate conditions including output power, current, and switching frequency based on the two characterization stages (low flux and high flux characterizations).

A. Low Flux in Situ Characterization

For the *in situ* measurement, inductance and quality factor of the test inductor were assessed using an impedance analyzer (HP 4194 A) prior to sacrificial copper layer etching, and subsequently at various times during the progression of the sacrificial layer etching, enabling assessment of the eddy current suppression. Note that the measurements at various stages of sacrificial layer etching are performed by removing the test inductors from the etchant, immersing them in deionized water. Then, the test inductor is returned to the etch solution for continued etching. Fig. 5 shows the inductance and the quality factor from the test inductor before and after the sacrificial copper layer removal from the nanolaminated CoNiFe cores. For this result, a pre-measured inductance and resistance of an air core inductor (i.e., wound bobbin without magnetic core) of nominally identical geometry were subtracted from a measured inductance and resistance of a magnetic core inductor (i.e., wound bobbin with magnetic core), thus the results are solely attributable to the

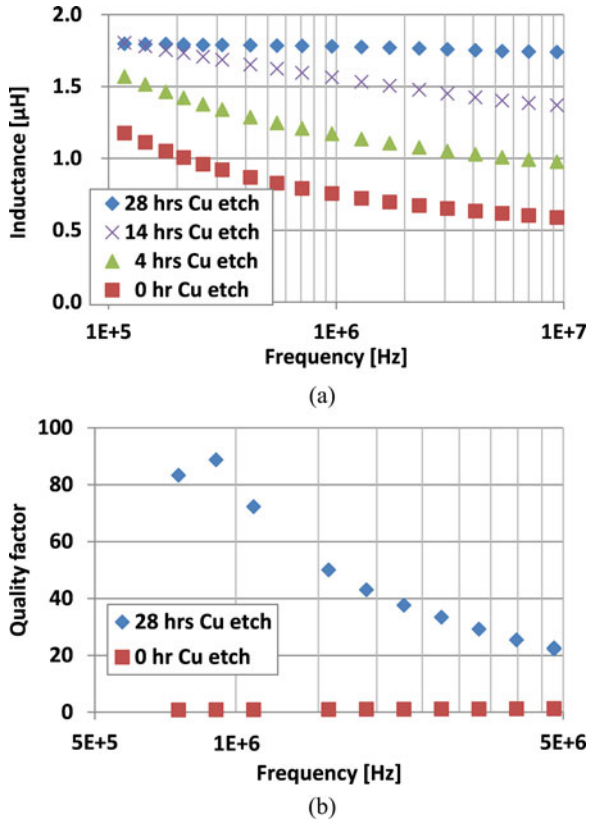

Fig. 5. Characterization of nanolaminated CoNiFe core before and after sacrificial copper layer etching. (a) Inductance and (b) quality factor.

magnetic core performance. Fig. 5(a) shows an example of measured inductance as a function of operation frequency parameterized by etching time. The test inductor possesses 36 turn windings around a nanolaminated CoNiFe core having outer diameter of 10 mm and inner diameter of 6 mm. Before sacrificial copper layers are etched, the nanolaminated CoNiFe core comprises 70 alternating pairs of CoNiFe and copper layers in which every layer is electrically connected causing significant eddy current flow throughout the bulk metallic medium since the total core thickness exceeds the skin depth of the material in the measured frequency region. Consequently, a significant inductance decrease as a function of operation frequency is observed as shown in Fig. 5(a). However, each CoNiFe lamination is electrically isolated after the removal of the sacrificial copper layers, demonstrating eddy current suppression. As a result, a constant inductance is observed as a function of operation frequency validating the complete sacrificial copper removal. The complete removal of the copper in the core is also verified by etching the cores without support holes in which the copper is etched only through the inner and outer peripheries of the toroidal core, until physical separation of the magnetic layers is observed. This experiment enables an estimation of complete copper etching time. Complete copper etching for cores having 10 mm outer diameter and 8 mm inner diameter occurs in approximately 24 h. As shown in Fig. 5(a), a copper etching time exceeding 24 h was utilized to ensure compete copper removal.

The measured quality factor of the nanolaminated CoNiFe core after copper removal approaches 80 at 1 MHz, whereas the quality factor before the copper removal is less than 2 in the measured frequency region. For comparison, a previously reported nanolaminated permalloy core with the same geometry shows a quality factor approaching 60 at 1 MHz after complete removal of the sacrificial copper layer [16].

B. High Flux Characterization

The superior saturation flux density of CoNiFe enables operation of nanolaminated CoNiFe cores with high peak flux densities (>0.1 T), which is challenging to achieve with commercial ferrite cores. In order to investigate the power losses of nanolaminated CoNiFe cores at HFHF, we adopted a magnetic material characterization method which has been proposed by Han *et al*. in 2008 [27]. The method relies on series resonance between a device under test (i.e., inductor with nanolaminated CoNiFe core) and a reference capacitor, enabling a calculation of core losses as a function of operation flux density as well as frequency. For the characterization, the test inductor is modeled as a series connection of an ideal inductance and two resistive elements ($R_{\rm cu}$ and $R_{\rm core}$) representing the coil and core losses. The reference capacitor is also regarded as a combination of ideal capacitance and resistance, and the capacitance should be carefully selected to resonate with the inductor at the desired measurement frequency.

During the measurement, the amplitude and the frequency of a sinusoidal input voltage, generated by a signal generator (Agilent 33120A) and an RF power amplifier (TOMCO), are precisely modulated to resonate the circuit at the desired flux density within the core. The output voltage from the reference capacitor, monitored by an oscilloscope (Tektronix TDS 2024C), and premeasured capacitance are used to calculate the current in the circuit ($I = V_{\rm out}/X_c$). The flux within the core is estimated from the voltage across the secondary pickup coil of the inductor using Faraday's law of induction. Note that all flux densities used in this paper represent peak flux density. Finally, the *LC* circuit operates as a purely resistive load at the resonant frequency allowing the calculation of power losses of the core as a product of the square of the circuit current (I^2) and core loss ($R_{\rm core}$). In this high flux characterization, premeasured resistances of the resonant capacitor, experimental PCB, and an air core inductor of nominally identical geometry were determined at the same frequency. These premeasured values were subtracted from the resistance of the inductors with the nanolaminated CoNiFe cores during the measurement so that the presented volumetric power losses are attributable to the core material alone.

Fig. 6 shows the volumetric power losses of a nanolaminated CoNiFe core comprising 70 layers of 500-nm-thick CoNiFe characterized in a 36-turn test inductor. To determine the volumetric loss, it is important to distinguish between the *total* core volume (i.e., the volume occupied by magnetic material and support holes), and the *magnetic* core volume, which is the volume occupied only by magnetic material (see Fig. 3). To determine the volumetric core loss, the measured loss is divided by the magnetic core volume, calculated by multiplying: 1) the core surface area that excludes the area of the support holes; 2) the thickness of a single lamination layer; and 3) the number of

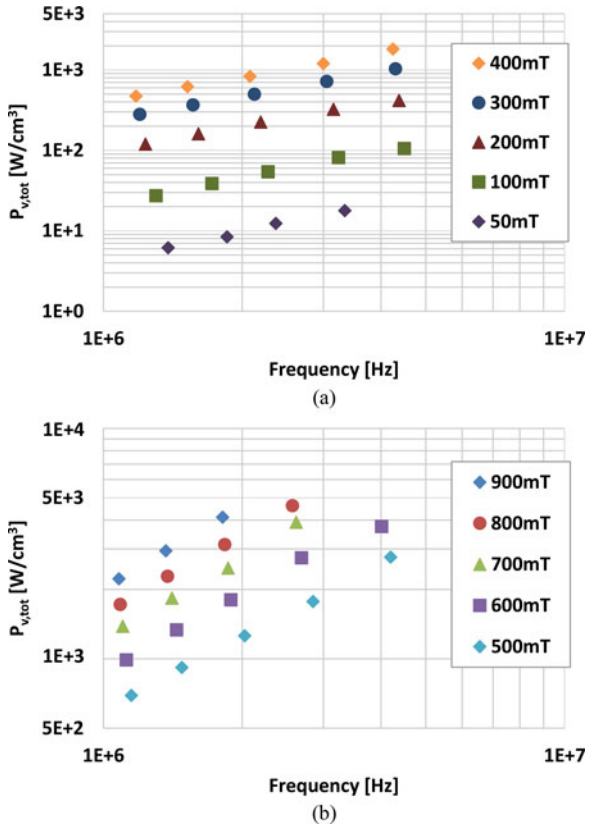

Fig. 6. Volumetric power losses of a nanolaminated CoNiFe core as a function of frequency up to 0.9 T peak flux density: (a) 0.05–0.4 T, (b) 0.5–0.9 T. Note that *y*-axis is in log scale.

layers. Calculated in this way, the total core volume of the 70 layers of 500-nm-thick CoNiFe core is 1.3496 mm^3. A similar distinction needs to be made when calculating the cross-sectional area of the core; however, in this case, the determination is more complex. The presence of the support holes causes a nonuniform flux distribution in the core, since the angular discretization of the support holes around the core results in some cross sections having support holes and some not having support holes. For the estimation of the cross-sectional area containing support holes, two extreme cases can be considered: 1) Assuming that magnetic flux flows through the entire cross section (i.e., cross section includes both the magnetic material and the support holes), the cross section area becomes 0.07 mm^2 (2 mm $\times$ 500 nm $\times$ 70 layer). 2) Assuming that magnetic flux flows only through the magnetic material (i.e., only the magnetic material is considered as a cross section), the cross section area becomes 0.05369 mm^2 (1.534 mm $\times$ 500 nm $\times$ 70 layer) since the support holes occupy 23.3% of the core surface area. Therefore, the effective cross-sectional area is between these two extreme cases. Case 1 (i.e., magnetic flux distribution across 0.07 mm^2 of area) was utilized for flux density calculations since it results in an overestimation of the volumetric power loss. Detailed dimensions of the nanolaminated CoNiFe core are presented in Table IV.

The high flux measurement was conducted at operation peak flux densities up to 0.9 T in the 1–5 MHz frequency range. The high operation peak flux density of 0.9 T is challenging to achieve with previously developed nanolaminated permalloy cores as well as commercial ferrite cores due to their intrinsic magnetic property (i.e., low saturation flux density). During high flux operation, the temperature variation of the core was measured using an infrared thermometer. Negligible temperature increase was observed up to operation peak flux density of 0.3 T without any thermal cooling. Also, without thermal cooling, the temperature increase reached 50 °C at 0.4 T. Above this flux level, convective cooling was employed during the highest operation peak fluxes over 0.5 T where the core temperature reached 100 °C implying that appropriate thermal cooling (e.g., convective cooling or heat sinking) may be required for the highest peak flux level operation.

Further investigation of the nanolaminated CoNiFe core was performed by decomposing the measured total volumetric power loss ($P_{V,\mathrm{tot}}$) into two categories: 1) volumetric hysteresis losses ($P_{V,\mathrm{hyst}}$) associated with magnetic domain motion; and 2) volumetric eddy current losses ($P_{V,\mathrm{eddy}}$) from the induced current with in the conducting medium due to time-varying magnetic flux [17], [18]. When the lamination thickness is below the skin depth, hysteresis losses increase with frequency (f) and eddy current losses increases with frequency square (f^2) [18], [28]. Since the lamination thickness (500 nm) is well-below the skin depth ($\sim$3 μm at 10 MHz), the total volumetric power losses of the nanolaminated CoNiFe core is analytically expressed as:

$$P_{V,\mathrm{tot}} = P_{V,\mathrm{hyst}} + P_{V,\mathrm{eddy}} = k_{\mathrm{hyst}} f + k_{\mathrm{eddy}} f^2 \qquad (6)$$

where k_{hyst} is the volumetric hysteresis loss coefficient and k_{eddy} is the volumetric eddy current loss coefficient. Although anomalous losses are ignored in (6), their effects will be distributed among the losses attributed to eddy currents and hysteresis, meaning that the losses measured by this technique are conservative estimates of the true losses due to eddy currents and hysteresis. Consequently, by plotting $P_{V,\mathrm{tot}}/f$ as a function of operation frequency, both coefficients (k_{hyst} and k_{eddy}) are obtained from the intercept and the slope of the graph, respectively. Thus, it can be considered that eddy current losses are suppressed if the graph shows a small slope. Fig. 7 shows $P_{V,\mathrm{tot}}/f$ of the nanolaminated CoNiFe core as a function of frequency parameterized by operation peak flux densities ranging from 0.1 to 0.9 T. The linear fitting lines are extracted from the measured data of each peak flux density showing nearly zero-degree slopes. Also, both coefficients indicate that volumetric eddy current losses are much lower than volumetric hysteresis losses, demonstrating that the eddy currents are suppressed in the nanolaminations of the core at the measured high frequencies and high flux densities.

Fig. 8 shows total volumetric power losses divided into hysteresis and eddy current losses at 1 MHz as a function of peak flux density, demonstrating that the total power losses are dominated by hysteresis losses, while eddy current losses are suppressed to approximately 1–3% of the total losses. Note that volumetric eddy current losses at lower peak flux densities (e.g., 0.1–0.4 T) are hardly seen in the graph meaning that the eddy current losses are suppressed to a negligible level. In order to further evaluate the correlation between the total volumetric

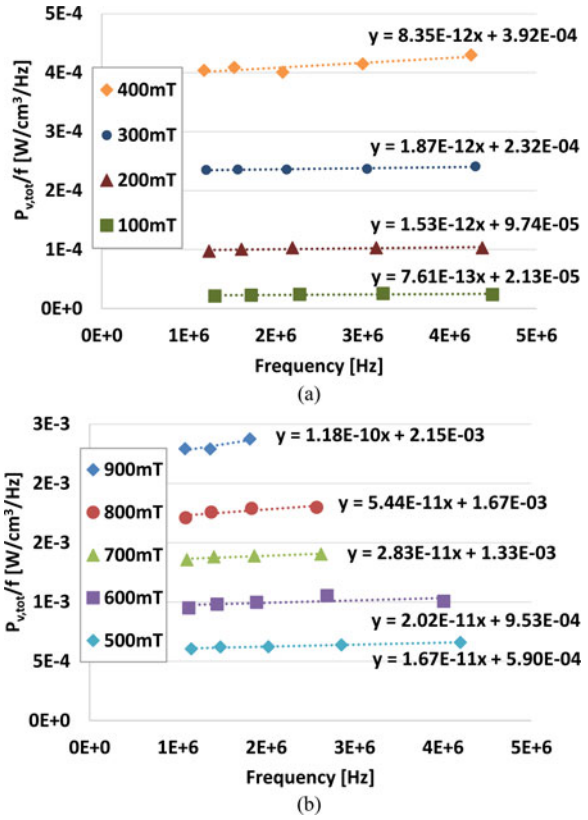

Fig. 7. Measured volumetric power losses over operation frequency up to 0.9 T peak flux density: (a) 0.1–0.4 T, (b) 0.5–0.9 T.

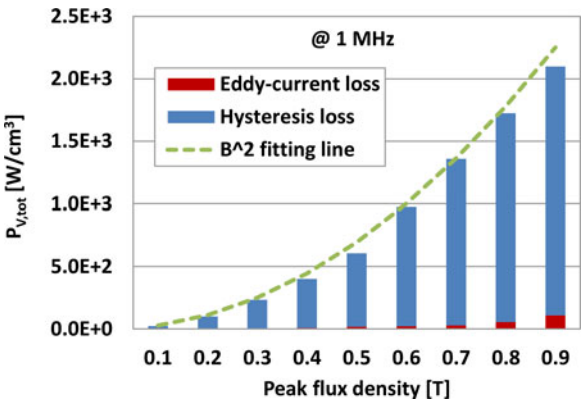

Fig. 8. Volumetric power losses of nanolaminated CoNiFe core divided into hysteresis and eddy current losses at 1 MHz as a function of peak flux density.

power losses of the nanolaminated CoNiFe core with operation peak flux density, a $B_{\rm peak}^2$ fitting line is also plotted in Fig. 8, demonstrating that measured volumetric power losses at 1 MHz correspond with a $B_{\rm peak}^2$ line.

In order to compare the high flux performance of a nanolaminated CoNiFe core with the previously developed nanolaminated permalloy core, the total volumetric power losses of both cores at 1 MHz as a function of peak flux densities ranging from 0.1 to 0.5 T are plotted in Fig. 9. Both cores comprise 70 layers of 500 nm-thick laminations with the same geometry. As shown in the graph, the nanolaminated CoNiFe core exhibits approximately 30% reduced total volumetric power losses at the same

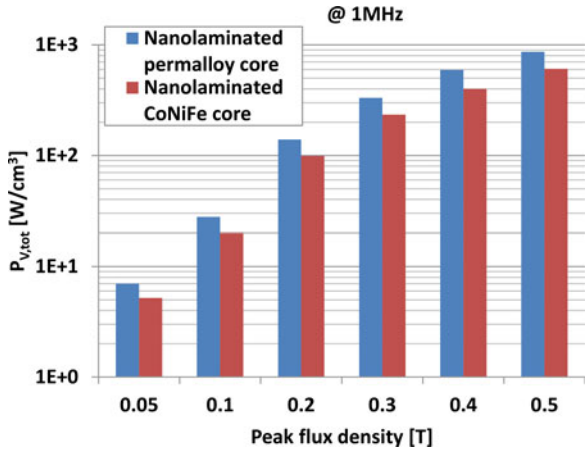

Fig. 9. Volumetric power losses of a nanolaminated CoNiFe core and a nanolaminated permalloy core at 1 MHz as a function of peak flux density. Note that y-axis is in log scale.

TABLE III
PROPERTIES OF COMMERCIAL MNZN FERRITES

Product	$P_{\rm vol}$ [W/cm³] (0.05 T, 1 MHz)	Bs [T]	Hc [Oe]	μ_i	ρ [Ω · m]
3F35 [30]	0.7	0.5	N/A	1400	10
3F45 [31]	0.3	0.42	N/A	900	10
N59 [32]	0.51	0.46	0.8	850	25
N49 [32]	0.56	0.46	0.7	1300	11
PC95 [33]	3.8 (0.1 T, 1 MHz)	0.53	9.5	3300	6
TP5B [34]	0.6	0.5	N/A	1000	9

flux levels compared to the nanolaminated permalloy core. Since eddy current losses of both the nanolaminated CoNiFe core and the nanolaminated permalloy core are suppressed to a negligible level, the reduced volumetric power losses of the nanolaminated CoNiFe core are mainly attributed to the lower hysteresis losses resulting from the lower coercivity of CoNiFe material.

For comparison, characteristics (e.g., saturation flux density and volumetric power loss) of several commercial MnZn ferrites that can be operated at low megahertz frequency are presented in Table III. These materials exhibit lower volumetric power losses than the nanolaminated CoNiFe core at 0.05 T peak flux density and 1 MHz frequency. Although these losses are lower than that of the CoNiFe cores at these relatively low flux densities, achieving ultracompactness in inductors and converters requires operation at much higher flux densities. The demonstrated operation peak flux density of the nanolaminated CoNiFe core of up to 0.9 T exceeds not only the operating flux density but also the saturation flux density of these ferrites. The volumetric power loss of the nanolaminated CoNiFe core, which is dominated by hysteresis loss, can be further reduced by introducing magnetic anisotropy [29] or changing the component and/or composition of the metallic alloy [24].

C. Characterization in DC–DC Converter

The 36-turn test inductor with a laminated CoNiFe core comprising 70 layers of 500-nm-thick laminations was operated in a

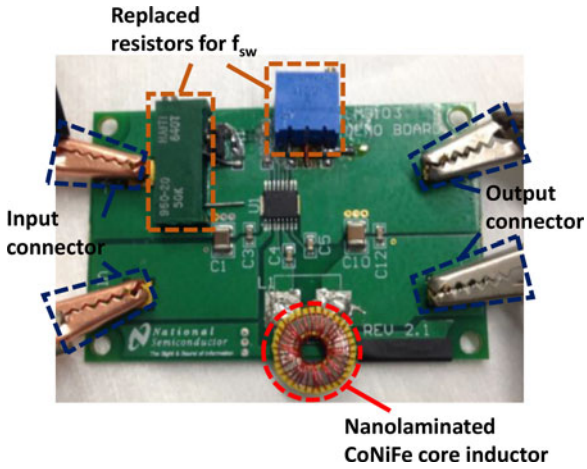

Fig. 10. Image of a dc–dc converter evaluation board with a 36-turn inductor with nanolaminated CoNiFe core.

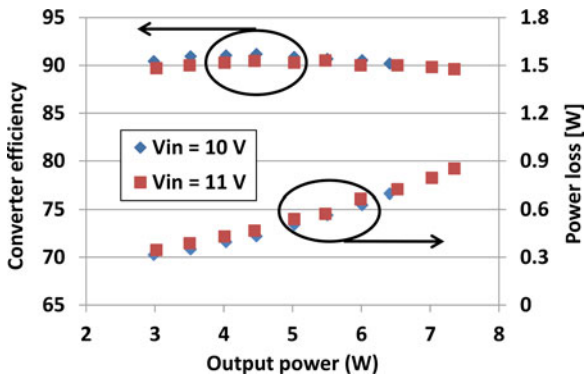

Fig. 11. Experimental measurements of dc–dc power converter performance tested with a nanolaminated CoNiFe core inductor. Converter efficiency and power loss as a function of output power.

dc–dc converter evaluation board (LM 3103, TI) by replacing a commercial inductor in the board with the test inductor as shown in Fig. 10. The details of the evaluation board are found in [35]. During the measurement, input voltages are higher than 10 V, and output voltage is fixed at 7 V with a switching frequency approximately 1.1 MHz. The converter efficiency and power loss of the converter with the test inductor as a function of output power range are shown in Fig. 11. Under the operated output power levels (3–8 W), the converter efficiencies were approximately 90% at a switching frequency approximately 1.1 MHz. The operation peak flux density of the core reaches 0.4 T during the measurement, which would be challenging to achieve with conventional ferrite cores.

It is tempting to correlate the core performance during the converter test with the high flux measurement results; however, care must be taken in this comparison because the current waveforms seen by the inductor in these two tests could be significantly different. The peak flux density of the core during converter operation is estimated as [36]

$$B_{\text{peak}} = \frac{(V_{\text{in}} - V_o) \cdot V_o}{2 \cdot V_{\text{in}} \cdot f_{\text{sw}} \cdot N \cdot A_c} \tag{7}$$

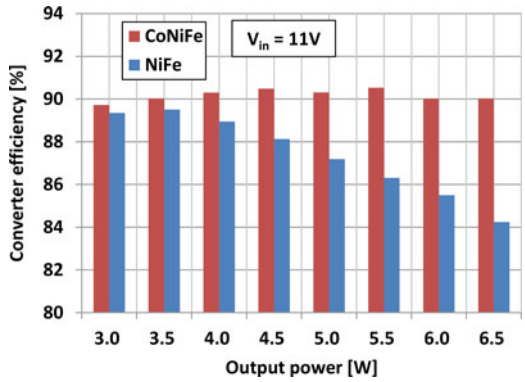

Fig. 12. Comparison of power converter performance tested with a nanolaminated CoNiFe core inductor and a nanolaminated permalloy core inductor. Converter efficiency at 11 V input as a function of output power.

where N is the number of inductor windings, and A_c is the cross-sectional area of the core. The volumetric core loss measured from the high flux characterization is approximately 400 W/cm^3 at 0.4 T peak as shown in Fig. 9. Since the volume of the nanolaminated CoNiFe core is 1.35e–9 m^3, the total core loss during the converter operation could be estimated as 0.54 W, exceeding the total converter power loss at low output power (<5 W) as shown in Fig. 11. However, such comparisons should be made with care, given the difference in inductor excitation waveforms between the HFHF and converter measurements, as well as the overestimation of power losses as discussed in Section IV-B.

Fig. 12 compares the converter efficiency as a function of the output power when the converter operates with the nanolaminated CoNiFe core and the same geometry nanolaminated permalloy core under input voltage of 11 V, output voltage of 7 V, and switching frequency of approximately 1.1 MHz. At the same output power levels, use of the nanolaminated CoNiFe core resulted in higher converter efficiency than use of the nanolaminated permalloy core as shown in the graph. Also, it is observed that the converter efficiency decreased as output power increased when the converter operated with a nanolaminated permalloy core, while the converter efficiency remained higher than 90% over the entire range of output power levels when it was operated with a nanolaminated CoNiFe core. The decreasing efficiency of the converter employing the nanolaminated permalloy core is caused possibly due to the saturation of the magnetic core. Considering the dc current of the inductor ($I_{\text{dc}} = V_{\text{out}}/R_{\text{out}}$) during the converter operation, together with the peak flux density in (7), it is estimated that the maximum peak flux density of the permalloy core at high output power levels (>5 W) is approaching 1 T, which is close to the saturation flux density (1.2 T) of the material. In this saturation region, magnetic material can exhibit nonlinear behavior (e.g., nonlinear permeability) [17], possibly resulting in unstable operation of the converter (e.g., altering switching frequency). Consequently, there can be increasing losses from the magnetic core as well as other components in the converter. This means that the nanolaminated permalloy core requires larger volume in order to operate the same power levels, demonstrating the

TABLE IV
COMPARISON OF NANOLAMINATED PERMALLOY AND CONIFE CORES

Inductor and core configuration		
Number of windings	36	
Core outer diameter	10 mm	
Core inner diameter	6 mm	
Number of support holes	200	
Total support hole area	11.7 mm^2	
Core surface area (excluding the area of the support holes)	38.56 mm^2	
Single layer thickness	500 nm	
Number of layers	70	
Total magnetic layer thickness	35 μm	
Effective core cross section area	0.0537 – 0.07 mm^2	
Magnetic core volume	1.3496 mm^3	
Total core volume	1.7593 mm^3	
Thin film property		
	Permalloy	**CoNiFe**
Saturation flux density	1.25 T	1.83 T
Coercivity force	1.5 Oe	0.5 Oe
Nanolaminated core		
Core peak quality factor	60 (@ 1 MHz)	80 (@ 1 MHz)
Effective permeability	$\sim$ 150	$\sim$ 200
Operation peak flux density	Up to 0.5 T	Up to 0.9 T
$P_{V,\mathrm{hyst}}$ (@1 MHz, 0.4 T)	566 W/cm^3	392 W/cm^3
$P_{V,\mathrm{eddy}}$ (@1 MHz, 0.4 T)	28.3 W/cm^3	8.35 W/cm^3
Converter test		
Input voltage	10–11 V	10–11 V
Output voltage	7 V	7 V
Output power	3–6.5 W	3–8 W
Switching frequency	1.05–1.3 MHz	1.05–1.1 MHz
Peak flux density of core	0.4 T	0.4 T
Converter efficiency	84$\sim$89%	90$\sim$91%

superior performance of the nanolaminated CoNiFe core over that of nanolaminated permalloy core for the compact dc–dc power conversion application.

The properties of both nanolaminated permalloy and CoNiFe cores ranging from intrinsic magnetic property to system level performance are compared in Table IV showing the superior properties of the nanolaminated CoNiFe core. Note that the core cross-sectional area of 0.07 mm^2 has been used for this paper.

V. CONCLUSION

This paper demonstrated the improved performance of nanolaminated CoNiFe magnetic cores in dc–dc power conversion applications, compared to the previously reported nanolaminated permalloy cores. These improvements were achieved by utilizing a new magnetic material, CoNiFe, that possesses advanced magnetic properties, while maintaining the overall magnetic volume the same. Based on a CMOS-compatible sequential electrodeposition technique, fabricated nanolaminated CoNiFe cores consisted tens to hundreds layers of 300–500-nm-thick laminations, demonstrating suppressed eddy current losses up to 10 MHz operating frequency and high peak flux density levels up to 0.9 T. The advanced intrinsic magnetic properties of CoNiFe (i.e., higher saturation flux density and lower coercivity) than permalloy resulted in three major improvements of the nanolaminated CoNiFe core when compared to the same configuration nanolaminated permalloy cores: 1) greater peak flux density operation (up to 0.9 T) due to the higher saturation flux density; and 2) approximately 30% reduced volumetric power loss at the same peak flux levels due to the lower coercivity; and 3) higher power level operation with increased efficiency ($\sim$90%) in dc–dc power converter. The high saturation flux density of CoNiFe, together with large number of nanorange magnetic layers enabled by sequential electrodeposition will enable the development of high power density, ultracompact magnetic components for dc–dc power conversion applications.

ACKNOWLEDGMENT

Microfabrication was carried out in part in the Georgia Tech's Institute for Electronics and Nanotechnology. Donation of evaluation boards from TI is gratefully acknowledged.

REFERENCES

[1] F. Waldron, R. Foley, J. Slowey, A. N. Alderman, B. C. Narverson, and S. C. O. Mathuna, "Technology roadmapping for power supply in package (PSiP) and power supply on chip (PwrSoC)," *IEEE Trans. Power Electron.*, vol. 28, no. 9, pp. 4137–4145, Sep. 2013.

[2] C. R. Sullivan, D. V. Harburg, J. Qiu, C. G. Levey, and D. Yao, "Integrating magnetics for on-chip power: A perspective," *IEEE Trans. Power Electron.*, vol. 28, no. 9, pp. 4342–4353, Sep. 2013.

[3] Q. Li, M. Lim, J. Sun, A. Ball, Y. Ying, F. C. Lee, and K. D. T. Ngo, "Technology roadmap for high frequency integrated dc–dc converter," in *Proc. IEEE 6th Int. Power Electron. Motion Control Conf.*, 2009, pp. 1–8.

[4] D. J. Perreault, J. Hu, J. Rivas, Y. Han, O. Leitermann, R. C. N. Pilawa-Podgurski, A. Sagneri, and C. R. Sullivan, "Opportunities and challenges in very high frequency power conversion," in *Proc. IEEE Appl. Power Electron. Conf. Expo.*, Feb. 2009, pp. 1–14.

[5] C. O'Mathuna, N. Wang, S. Kulkarni, and S. Roy, "Review of integrated magnetic for power supply on chip (PwrSoC)," *IEEE Trans. Power Electron.*, vol. 27, no. 11, pp. 4799–4816, Nov. 2011.

[6] D. S. Gardner, G. Schrom, P. Hazucha, F. Paillet, T. Karnik, and S. Borkar, "Integrated on-chip inductor with magnetic films," *IEEE Trans. Magn.*, vol. 43, no. 6, pp. 2615–2617, Nov. 2007.

[7] K. Ikeda, K. Kobayashi, and M. Fujimoto, "Multilayer nanogranular magnetic thin films for GHz applications," *J. Appl. Phys.*, vol. 92, no. 9, pp. 5395–5400, 2002.

[8] D. Flynn, A. Toon, L. Allen, R. Dhariwal, and M. P. Y. Desmulliez, "Characterization of core materials for microscale magnetic components operating in the megahertz frequency range," *IEEE Trans. Magn.*, vol. 43, no. 6, pp. 3171–3180, Jul. 2007.

[9] J. Y. Park and M. G. Allen, "Integrated elecgtroplated micromachined magnetic devices using low temperature fabrication processes," *IEEE Trans. Electron. Packag. Manufact.*, vol. 23, no. 1, pp. 48–55, Sep. 2000.

[10] R. Meere, T. O'Donnell, H. J. Bergveld, N. Wang, N. Achotte, F. Rhen, and C. O'Mathuna, "Analysis of micro-inductor performance in a 20–100 MHz DC/DC converter," *IEEE Trans. Power Electron.*, vol. 24, no. 9, pp. 2212–2218, Sep. 2009.

[11] C. H. Ahn and M.G. Allen, "A comparison of two micromachined inductors (bar-type and meander-type) for fully integrated boost DC/DC power converters," in *Proc. IEEE 9th Appl. Power Electron. Conf.*, Feb. 1994, vol. 1, pp. 10–16.

[12] J. W. Park, P. F. Cros, M. G. Allen, and Y. K. Yoon, "Magnetic inductor core and inductor and methods for manufacturing same," U.S. Patent 2004/0 164 839 A1, 2004.

[13] J. W. Park, "Core lamination technology for micromachined power inductive components," Ph.D. dissertation, Dept. Electr. Comput. Eng., Georgia Institute of Technology, Atlanta, GA, USA, Dec. 2003.

[14] J. Kim, J.-K. Kim, M. Kim, F. Herrault, and M. G. Allen, "Microfabrication of toroidal inductors integrated with nanolaminated ferromagnetic metallic cores," *J. Micromech. Microeng.*, vol. 23, pp. 114006-1–114006-9, Oct. 1998.

[15] M. Kim, F. Herrault, J. Kim, J. K. Kim, and M. G. Allen, "Monolithically-fabricated laminated inductors with electrodeposited silver windings," in *Proc. IEEE 26th Int. Conf. Micro Electro Mech. Syst.*, Jan. 2013, pp. 873–876.

[16] J. Kim, M. Kim, P. Galle, F. Herrault, R. Shafer, J. Y. Park and M. G. Allen, "Nanolaminated permalloy core for high-flux, high-frequency ultracompact power conversion," *IEEE Trans. Power Electron.*, vol. 28, no. 9, pp. 4376–4383, Sep. 2013.

[17] G. Bertotti, *Hysteresis in Magnetism*. London, U.K.: Academic, 1998.

[18] J. P. Barranger, *Hysteresis and Eddy-Current Losses of a Transformer Lamination Viewed as an Application of the Poynting Theorem*. Washington, DC, USA: NASA, 1965.

[19] N. Wang, T. O'Donnell, S. Roy, P. McCloskey, and C. O'Mathuna, "Micro-inductors integrated on silicon for power supply on chip," *J. Magn. Magn. Mater.*, vol. 316, no. 2, pp. e233–e237, Sep. 2007.

[20] J. Y. Park, "Packaging-compatible micromachined magnetic devices: Integrated passive components and modules," Ph.D. dissertation, Dept. Electr. Comput. Eng., Georgia Institute of Technology, Atlanta, GA, USA, Dec. 1997.

[21] J. Y. Park and M. G. Allen, "Development of magnetic materials and processing techniques applicable to integrated micromagnetic devices," *J. Micromech. Microeng.*, vol. 8, no. 4, pp. 307–316, Dec. 1998.

[22] T. E. Mastouli, J. P. Laur, J. L. Sanchez, M. Brunet, D. Bourrier, and M. Dilhan, "Micro-inductors integrated on silicon for DC-DC converters," *Proc. SPIE, Micromach. Microfab. Process Technol.*, vol. 6882, pp. 68820A1–68820A8, Feb. 2008.

[23] T. Osaka, M. Takai, K. Hayashi, K. Ohashi, M. Saito, and K. Yamada, "A soft magnetic CoNiFe film with high saturation magnetic flux density and low coercivity," *Nature Mater.*, vol. 392, no. 23, pp. 796–798, Apr. 1998.

[24] X. Liu, G. Zangari, M. Shamsuzzoha, "Structural and magnetic characterization of electrodeposited high moment FeCoNi films," *J. Electrochem. Soc.*, vol. 150, no. 3, pp. C159–C168, 2003.

[25] Y. Sverdlov, Y. Rosenberg, Y. I. Rozenberg, R. Zmood, R. Erlich, S. Natan, and Y. S. Diamand, "The electrodeposition of cobalt-nickel-iron high aspect ratio thick film structures for magnetic MEMS applications," *Microelectron. Eng.*, vol. 76, nos. 1–4, pp. 258–265, Oct. 2004.

[26] F. Herrault, W. P. Galle, R. H. Shafer, and M. G. Allen, "Electroplating-based approaches for volumetric nanomanufacturing," in *Proc. Tech. Dig. Technol. Future Micro-Nano Manuf.*, 2011, pp. 71–74.

[27] Y. Han, G. Cheung, A. Li, C. R. Sullivan, and D. J. Perreault, "Evaluation of magnetic materials for very high frequency power applications," in *Proc. IEEE Power Electron. Spec. Conf.*, Jun. 2008, pp. 4270–4276.

[28] J. Lammeraner and M. Stafl, *Eddy Current*. London, U.K.: Iliffe, 1966.

[29] T. Masai and Y. Kitamoto, "Effect of slit patterning perpendicular to magnetic easy axis in thin film inductors," *IEEE Trans. Magn.*, vol. 44, no. 11, pp. 3871–3874, Nov. 2008.

[30] (2008). [Online]. Available: http://www.ferroxcube.com/FerroxcubeCorporateReception/datasheet/3f35.pdf.

[31] (2008). [Online]. Available: http://www.ferroxcube.com/FerroxcubeCorporateReception/datasheet/3f45.pdf.

[32] (2006). [Online]. Available: http://www.thierry-lequeu.fr/data/SIFERRIT.pdf.

[33] (2014). [Online]. Available: http://product.tdk.com/en/catalog/datasheets/ferrite_mn-zn_material_characteristics_en.pdf.

[34] (2006). [Online]. Available: http://tdgcoreen.sx47.80data.net/upload/product/2.pdf.

[35] (2013). [Online]. Available: http://www.ti.com/lit/ds/symlink/lm3103.pdf.

[36] D. Hart, *Power Electronics (Ch.6)*. New York, NY, USA: McGraw-Hill, 2011.

Jooncheol Kim received the B.S. degree in electrical engineering from the Soongsil University, Seoul, Korea, in 2009, and the M.S. degree in electrical and computer engineering from the Georgia Institute of Technology, Atlanta, GA, USA, in 2011. He has joined a research group of Professor M. G. Allen in 2010 to receive the Ph.D. degree in ECE.

His current research focuses on developing passive and active devices using microfabrication technologies for sensors and power converters.

Minsoo Kim received the B.S. and M.S. degrees in electrical and computer engineering from Seoul National University, Seoul, Korea, in 2006 and 2008, respectively. Since 2010, he has been working toward the Ph.D. degree in Georgia Tech, Atlanta, GA, USA.

Until 2009, he was with the Korea Institute of Industrial Technology, and was involved in the research on inkjet-printed electronics. His current research interests include 3-D microfabrication technology based on multilayer electrodeposition for the realization of a variety of passive and active devices.

Florian Herrault (SM'14) received the B.S. and M.S. degrees in physics and materials science from the National Institute of Applied Sciences,Toulouse, France, in 2003 and 2005, respectively, and the Ph.D. degree in electrical and electronics engineering from the University of Toulouse, Toulouse, in 2009.

From 2009 to 2013, he was a Research Engineer with the MicroSensors and MicroActuators Group (Georgia Institute of Technology), and acted as the group's Deputy Director. He is currently a Member of the Technical Staff at HRL Laboratories developing advanced microfabrication-based packaging technologies for millimeter-wave components. His research interests include integrated magnetics for power supplies on a chip and MEMS-based biomedical implants.

Dr. Herrault has been a Member of the technical program committee and a session Cochair for the International Workshop on Power Supply on Chip 2010 and 2012, the International Workshop on Micro- and Nanotechnology for Power Generation and Energy Conversion Applications 2012 and 2013, and the Solid-State Sensors, Actuators, and Microsystems Workshop 2014.

Jae Y. Park (M'95) received the Ph.D. degree in electrical and computer engineering from the Georgia Institute of Technology, Atlanta, GA, USA, in 1997.

After graduation, he was with the Georgia Institute of Technology as a Research Engineer for two years. He also was with the Microsystem group in the LG Electronics Institute of Technology as a Team leader of RF and power MEMS research for six years. In September 2004, he joined the faculty member of the Department of Electronic Engineering in Kwangwoon University, Seoul, Korea. He has published more than 200 journal articles and conference proceedings and filed more than 100 patents. His current research interests include optical MEMS devices, microsystem packaging (wafer level packaging, PCB embedded passives, circuits, and modules, system on packaging), nonenzymatic electrochemical bio and environmental sensors, energy harvesting and storage devices, and RF MEMS devices.

Mark G. Allen (M'88–SM'04–F'11) received the B.A. degree in chemistry, the B.S.E. degree in chemical engineering, and the B.S.E. degree in electrical engineering from the University of Pennsylvania, Philadelphia, PA, USA, the S.M. degree from the Massachusetts Institute of Technology, Cambridge, MA, USA, and the Ph.D. degree from the same university in 1989.

In 1989, he joined the faculty of the School of Electrical and Computer Engineering, Georgia Institute of Technology, Atlanta, GA, USA, ultimately holding the rank of Regents' Professor and the J.M. Pettit Professorship in Microelectronics, as well as a joint appointment in the School of Chemical and Biomolecular Engineering. In 2013, he left Georgia Tech to become the Alfred Fitler Moore Professor of Electrical and Systems Engineering and the Scientific Director of the Singh Nanotechnology Center at the University of Pennsylvania. His research interests include the development and the application of new micro- and nanofabrication technologies, as well as MEMS.

Dr. Allen was an Editor-in-Chief of the *Journal of Micromechanics and Microengineering*, and was a previous Cochair of the IEEE/ASME Microelectromechanical Systems Conference.